Nuclear structure effects of the nuclei ^{152,154,156}Dy at high excitation energy and large angular momentum

V. Martin
Análisis Numérico, Facultad de Informática, Universidad Politécnica de Madrid, E-28660 Madrid, Spain

J.L. Egido
Departamento de Física Teórica C-XI, Universidad Autónoma de Madrid, E-28049 Madrid, Spain
(Received 3 December 1993; revised manuscript received 22 September 1994)

Using the finite-temperature Hartree-Fock-Bogoliubov formalism we analyze the properties of the nuclei ^{152,154,156}Dy at the quasicontinuum region from $I = 0\hbar$ to $70\hbar$ and excitation energy up to approximately 16 MeV. We discuss energy gaps, shapes, moments of inertia, and entropy among others. The role of shape fluctuations is studied in the frame of classical statistics and we find large effects on several observables. A very rich structure is found in terms of excitation energy and angular momentum.

PACS number(s): 21.10.Re, 21.10.Ky, 21.60.Jz, 27.70.+q

I. INTRODUCTION

The experimental analysis of discrete γ rays has led in the last years to a renaissance of nuclear structure physics. Many new phenomena have been discovered, challenging both experimental and theoretical physicists. The next challenge, however, is to come in the near future when the new crystal ball detectors are in full production. This will be, probably, the era of the quasicontinuum, the 10 MeV broadband over the yrast line. We have obtained an indication of the phenomena to be discovered there with the example of the damping of rotational motion [1,2]. But many others, such as shape changes and the superfluid-normal fluid phase transition, are expected — the most interesting ones will be unexpected, though.

The study of the quasicontinuum is difficult from the theoretical and from the experimental point of view. On the theoretical side we do not know much about this region (see [3,4] for recent reviews on hot nuclei). We do not know, for example, the level densities, the order of magnitude of the reduced matrix elements for transition probabilities, the relevance of the residual interaction beyond the mean field, etc. The high level density, on the other hand, allows the introduction of a temperature concept to perform calculations with the grand canonical ensemble within the mean-field approximation. So far, most of the temperature-dependent calculations have been done within the Hartree-Fock (HF) [5,6], Hartree-Fock-Bogoliubov (HFB) [7], and Woods-Saxon plus Strutinsky methods (see [8] and references therein). These approximations have been generalized to high angular momentum for separable forces (pairing plus quadrupole) type [9–11] and the Woods-Saxon potential. We lack, however, calculations with effective forces (Skyrme-like) at high angular momentum. Recently, the Landau theory of phase transitions [12,13] has been also applied to the study of nuclear properties.

Finite-temperature (FT) mean-field calculations have been done for several nuclei, and there one finds sharp phase transitions in spite of the finite size of the atomic nuclei. It was soon recognized [14], however, that the inclusion of fluctuations around the self-consistent mean-field solution would wash out these phase transitions. The fluctuations are included within the framework of classical statistics; since they are very CPU-time consuming, there are few such calculations. There are some calculations [15,16] but to date we do not have any systematic study. The interesting question remains whether the experimentalists have found some hints about these phase transitions or some remnants of it in cases where they are smeared out. Recently, the collective $E2$ strength in the quasicontinuum has been measured in Argonne [17,18] for the nuclei ^{152}Dy, ^{154}Dy, and ^{156}Dy at different energies. They found a distinctive spectrum in ^{154}Dy which they interpret as caused by the large fluctuations expected in a smeared-out shape transition. The purpose of this paper is to make a complete study of these nuclei up to high excitation energy and large angular momentum using the FTHF and FTHFB approximations and the Hamiltonian of pairing-plus-quadrupole model. A first analysis of these nuclei has been performed within the Landau theory by Alhassid [19]. These nuclei are transitional and we expect, therefore, fluctuations around the self-consistent minima to be important even at very low temperatures. At zero temperature we have quantum fluctuations; at nonzero temperature we have in addition thermal fluctuations. To consider both of them in realistic calculations is for the moment nonfeasible besides the fact that at moderately high temperatures we expect thermal ones to play the fundamental role. Thermal fluctuations in the collective parameters were first considered by Moretto [14] (for the pairing gap parameter) and later on for the shape parameters by several authors [20,21]. We shall include the last ones in our study.

The magnitude of this project together with the success of separable forces makes it necessary that we perform our study with the pairing-plus-quadrupole force. This force has been widely used, especially within the configuration space and parametrization of Baranger and

 ©1995 The American Physical Society

Kumar [22]; it has been also used at high spin [23,24] and finite temperature [9,11] with considerable success. Separable forces, however, have never been used to describe superdeformation, a shape that has been measured in the Dy region [25]. Although we are not primarily interested in this work in the description of superdeformed shapes, in order to be as realistic as possible, we tried to generalize this model to include the superdeformed minimum. We have tried straightforward changes: included more shells, shifted single-particle levels, changed the force constants, etc. We have not been able, however, within the philosophy of the Baranger-Kumar model to describe the shape coexistence that appears at ^{152}Dy. This is a nonexpected aspect of the separable forces and we believe that more work in this direction should be done. It does not appear so surprising, however, when one thinks that in the Landau theory of Alhassid *et al.* they do not obtain superdeformation, either, if they stop the expansion in the shape parameters at the quartic order.

The paper is organized as follows. In Sec. II the underlying theory is examined. In Sec. III the numerical results are discussed, in Sec. III A the self-consistent solutions and in Sec. III B with the inclusion of fluctuations. The paper ends with the conclusions.

II. THEORY

The mean-field approximation has been used in nearly all microscopic investigations of states near the yrast line [26,23,24], where it works very well. The extension to finite temperatures likewise has been very successful [27,9–11].

To derive these equations [4] one resorts to the variational principle of maximum entropy, which means that we have to maximize the entropy S under the constraint of constant average values of the energy E, particle number N, and angular momentum J. This is equivalent to the minimization of the thermodynamical potential

$$\Omega(\lambda,\omega,T) = E - \lambda N - \omega J - TS , \tag{1}$$

with the Lagrange multipliers λ, ω, and T determined by the average particle number N, angular momentum $J = \langle \hat{J}_x \rangle_T = \sqrt{I(I+1)}$, and energy E. These quantities are the ensemble average (thermal average) defined by

$$\langle \hat{\mathcal{O}} \rangle_T = \mathrm{Tr}(\hat{D}\hat{\mathcal{O}}) , \tag{2}$$

with $\hat{\mathcal{O}}$ an arbitrary operator and $\hat{D}$ the density operator. In the mean-field approximation this operator is approximated by

$$\hat{D}_0 = \frac{e^{\hat{K}/T}}{Z_0} , \tag{3}$$

where $\hat{K}$ is the most general Hermitian single-particle operator, to be determined by the variational principle, and Z_0 is the partition function.

In mean-field theories knowledge of the density matrix allows the evaluation of expectation values. The single-particle density matrix $\mathcal{R}$ in the HFB theory is defined as the thermal average

$$\mathcal{R} = \begin{pmatrix} \langle \alpha^\dagger_{m'} \alpha_m \rangle_T & \langle \alpha_{m'} \alpha_m \rangle_T \\ \langle \alpha^\dagger_{m'} \alpha^\dagger_m \rangle_T & \langle \alpha_{m'} \alpha^\dagger_m \rangle_T \end{pmatrix} , \tag{4}$$

where the index m labels the states of the configuration space; in the particle basis it has the form

$$\mathcal{R} = \begin{pmatrix} \rho & \kappa \\ -\kappa^* & 1-\rho^* \end{pmatrix} . \tag{5}$$

The relation between both bases is given by the Bogoliubov transformation

$$\alpha^\dagger_m = \sum_k U_{km} c^\dagger_k + V_{km} c_k . \tag{6}$$

The matrix elements of the matrix $\mathcal{R}$ are most easily evaluated in a basis of operators $\alpha_m, \alpha^\dagger_m$ in which the operator $\hat{K}$ of Eq. (3) is diagonal. In this basis the matrix $\mathcal{R}$ is also diagonal, its matrix elements being the quasiparticle occupation numbers; they are given by [4]

$$f_m = \langle \alpha^\dagger_m \alpha_m \rangle_T = \frac{1}{e^{k_m/T}+1} . \tag{7}$$

In an arbitrary basis, we obtain for the quasiparticle density matrix

$$\mathcal{R} = \frac{1}{e^{\mathcal{K}/T}+1} , \tag{8}$$

the supermatrix $\mathcal{K}$ being given by [4]

$$\mathcal{K} = \begin{pmatrix} K^{(11)} & K^{(20)} \\ -K^{(20)*} & -K^{(11)*} \end{pmatrix} . \tag{9}$$

$K^{(11)}$ and $K^{(20)}$ are the matrices representing the 11 and 20 parts of a one-body operator in the quasiparticle basis.

Now we are in position to calculate the expectation values appearing in Eq. (1). They can be evaluated with the Wick theorem; they turn out to be a functional of the density

$$E[\mathcal{R}] = \mathrm{Tr}(\epsilon\rho) + \frac{1}{2}\mathrm{Tr}(\Gamma\rho) - \frac{1}{2}\mathrm{Tr}(\Delta\kappa^*) , \tag{10}$$

with the average field

$$\Gamma_{kk'} = \sum_{ll'} v_{kl'k'l}\rho_{ll'} \tag{11}$$

and the pairing field

$$\Delta_{kk'} = \sum_{l<l'} v_{kk'll'}\kappa_{ll'} . \tag{12}$$

Before we can apply the variational principle, we also have to express the mean-field approximation for the entropy S in terms of the density $\mathcal{R}$; it is given by [4]

$$S[\mathcal{R}] = -\mathrm{Tr}(\mathcal{R}\ln\mathcal{R}) = -\mathrm{Tr}\left[\rho\ln\rho + (1-\rho)\ln(1-\rho)\right] . \tag{13}$$

Once we have expressed all quantities entering into (1) in

terms of the matrix density we can apply the variational principle to determine the density $\mathcal{R}$. The result is

$$\mathcal{R} = \frac{1}{e^{\mathcal{H}/T}+1}, \tag{14}$$

where

$$\mathcal{H} = \begin{pmatrix} h & \Delta \\ -\Delta^* & -h^* \end{pmatrix}, \tag{15}$$

with

$$h = \frac{\partial E'}{\partial \rho} = \epsilon - \lambda + \Gamma - \omega j_x, \qquad \Delta = \frac{\partial E'}{\partial \kappa}, \tag{16}$$

is a generalized single-particle operator depending on the density: $\mathcal{H} = \mathcal{H}(\mathcal{R})$ and $E' = E - \lambda N - \omega J$. That means that in the stationary system the operator $\hat{K}$ characterizing the statistical operator in the mean field is just given by the Hartree-Fock-Bogoliubov (HFB) approximation to the many-body Hamiltonian. We, therefore, have to solve the temperature-dependent HFB equations

$$\begin{pmatrix} h & \Delta \\ -\Delta^* & -h^* \end{pmatrix} \begin{pmatrix} U \\ V \end{pmatrix}_m = \begin{pmatrix} U \\ V \end{pmatrix}_m E_m \tag{17}$$

in order to calculate the HFB wave functions

$$\mathcal{W} = \begin{pmatrix} U & V^* \\ V & U^* \end{pmatrix} \tag{18}$$

and the densities

$$\begin{aligned} \rho &= U f U^\dagger + V^*(1-f)V^T, \\ \kappa &= U f V^\dagger + V^*(1-f)U^T, \end{aligned} \tag{19}$$

where f_m and $1 - f_m$, as mentioned, are the eigenvalues of $\mathcal{R}$. Equation (17) is usually solved by an iterative procedure which provides us with the self-consistent solution characterized by ρ and κ. In the mean-field approximation the single-particle degrees of freedom are fully taken into account by their own ansatz and the collective ones by the breakdown of the rotational invariance in the space associated with the corresponding symmetry, i.e., deformation with coordinate space and the particle number with the associated gauge space. If we denote our collective parameters by α, we can conclude that the solution of the HFB equations is given by $\rho(\alpha_0)$ and $\kappa(\alpha_0)$.

To go beyond mean-field theory we have to take into account, at zero temperature, quantum fluctuations around the mean-field values. At finite temperatures we have, in addition, statistical (or thermal) fluctuations, i.e., the incoherent averaging over many single-particle densities based on mean fields with different deformation parameters α. According to Landau [28] the probability for a certain value α of the deformation is characterized by the free energy $F(\alpha; I, T)$ of the system with this average deformation α,

$$p(\alpha; I, T) \propto e^{-F(\alpha;I,T)/T}, \tag{20}$$

with $F(\alpha; I, T) = E(\alpha; I, T) - T\,S$.

Using classical statistics, therefore, the ensemble average of an observable O is given by

$$\overline{O}(I,T) = \frac{\int O(\alpha; I, T)\, e^{-F(\alpha;I,T)/T} D[\alpha]}{\int D[\alpha]\, e^{-F(\alpha;I,T)/T}}, \tag{21}$$

with $O(\alpha; I, T)$ the thermal expectation value of the operator O calculated for the system with the deformation α [see Eq. (2)] and $D[\alpha]$ is the volume element in deformation space.

Two volume elements have been used in the past in the numerical applications. The first one takes into account all five quadrupole degrees of freedom $\alpha_{2\mu}$ [12,13]; the volume element is given in this case by $D[\alpha] = \prod_\mu d\alpha_{2\mu} = \beta^4 |\sin 3\gamma| d\beta d\gamma d\Omega$. If the fluctuations in the orientation of the nucleus are not considered, $d\Omega$ must be omitted. The second approach [20,21] starts from the intrinsic system point of view, taking into account only the fluctuations associated with the (β, γ) degrees of freedom; the volume element is given by $\beta d\beta d\gamma$. Goodman [29] has performed model calculations with both metrics. Theoretically, the phase space associated with the five degrees of freedom is more appropriate. In the calculations of this paper we use $D[\alpha] = \beta^4 |\sin 3\gamma| d\beta d\gamma$.

The standard deviation of $\hat{O}$ is given by

$$\sigma(O) = (\Delta O)^2 = \sqrt{\overline{\hat{O}^2} - \left[\overline{\hat{O}}\right]^2}. \tag{22}$$

The reduced transition probability $B(E2)$ along a rotational band from initial state I to final state $I-1$ is given by [30]

$$\begin{aligned} B(E2, I \to I-2) &= \sum_i p_i \, |\langle i|Q_{2-2}|i\rangle|^2 \\ &= \left| \sum_i p_i \, \langle i|Q_{2-2}|i\rangle \right|^2 \\ &\quad + \sum_m f_m \, (1-f_m) \, (Q^{11}_{2-2})^2_{mm}. \end{aligned} \tag{23}$$

p_i is the thermal occupation probability of configuration i and Q^{11}_{2-2} is the 11 part of the quadrupole operator Q_{2-2} in the quasiparticle representation.

For a realistic evaluation of the different observables entering into the electromagnetic decay of a hot nucleus we use the configuration space and the effective interaction of Kumar and Baranger [22]. The basic ingredient of the Hamiltonian is the pairing-plus-quadrupole force

$$H = \varepsilon - \frac{1}{2}\chi \sum_\mu Q^\dagger_{2\mu} Q_{2\mu} - G_P P^\dagger_P P_P - G_N P^\dagger_N P_N, \tag{24}$$

where ε are the spherical single-particle energies, $Q_{2\mu}$ are the quadrupole operators symmetrized with respect to the Goodman symmetry [31], and the operators P_P (P_N) create proton (neutron) Cooper pairs. The configuration space contains the spherical oscillator shells with the principal quantum numbers $N = 4$ and 5 for pro-

tons and $N = 5$ and 6 for neutrons. The force constants χ, G_P, and G_N and further details can be found in Ref. [22]. The single-particle energies, with the exception of the $\pi h_{11/2}$ level which was shifted in 0.1 MeV — as recommended in Refs. [32,33] — were also taken from Ref. [22]. Concerning the adequateness of the Baranger-Kumar configuration space at large angular momentum and high excitation energy, it has been shown by Goodman [34] that for temperatures below 1.0 MeV and small spins the space is big enough. Above 1.5 MeV one should add the $\pi i_{13/2}$ and $\nu j_{15/2}$ levels of the upper shells. At large angular momentum and high temperature there is not a systematic study; however, since we are mainly interested in the quasicontinuum region (which usually corresponds to temperatures below 0.8 MeV), we do not expect that the inclusion of these levels would affect our main conclusions.

In the actual calculations we proceed as follows. First the cranked finite-temperature Hartree-Fock equations are solved for fixed temperature and angular momentum by minimizing the grand potential

$$\Omega(I,T) = E - \lambda N - \omega J - T S , \qquad (25)$$

with the parameters λ and ω determined by the constraints

$$\langle \hat{N} \rangle_T = N_0, \qquad J = \langle \hat{J}_x \rangle_T = \sqrt{I(I+1)}, \qquad (26)$$

with N_0 the proton (neutron) number.

To take into account the fluctuations around the values (β_0, γ_0) of the self-consistent solution we now minimize the $\Omega(I,T)$ for constant values of (β, γ). We have used a grid of β values ranging from 0.05 up to 0.6, with a step size of 0.05 and γ values ranging from $-60°$ up to $120°$ with a step size of $10°$. This provided us with surfaces $F(\beta,\gamma;I,T) = E(\beta,\gamma;I,T) - T\ S$ for fixed values of (I,T) to evaluate the average values and the standard deviation of any operator as given by Eqs. (21) and (22), respectively.

III. RESULTS

In this section we present the results of two types of calculations. The first one is based on the self-consistent FTHFB approximation; i.e., we take into account the pairing correlations but we do not consider any type of thermal fluctuations around the self-consistent minima. In the second one we neglect the pairing correlations (i.e., we solve the FTHF equations) but we consider shape fluctuations in the way mentioned at the end of the last section. We do not consider pairing correlations in the calculation with shape fluctuations because in a study over such a extended region in the E-I plane the CPU time will increase beyond reasonable limits.

A. Self-consistent solution of the FTHFB equations

In Fig. 1 we show the internal energy as a function of the temperature for constant I values; in this figure the energy origin has been arbitrarily set for $I = 2\hbar$, $T = 0$ MeV. At low spins ($I < 20\hbar$) we observe a rather sudden increase of the energy, especially for ^{152}Dy, for $T > 0.5$ MeV. It has its origin in a combined effect of the pairing collapse and temperature-induced shape changes, which we will discuss in the following. At higher angular momenta ($I > 40\hbar$), the pairing energy is either zero or very small and the centrifugal forces make it harder for the temperature to change nuclear shape. As a consequence, the curves in Fig. 1 for ($I > 40\hbar$) are nearly parallel. From this figure one can find out, approximately, the equivalence between energy and temperature.

In Fig. 2 we present contour plots of the self-consistent gap parameter for constant temperatures as a function of the angular momentum for the nuclei ^{152}Dy, ^{154}Dy, and ^{156}Dy. We observe a pairing collapse as a function of the angular momentum ($I = 18\hbar, 14\hbar$, and $16\hbar$ for neutrons, and $40\hbar, 46\hbar$, and $42\hbar$ for protons for the three nuclei in the mentioned order) as well as a pairing collapse as a function of the temperature (at $T = 0.7, 0.6$, and 0.6 MeV for the neutron system and 0.9, 0.8, and

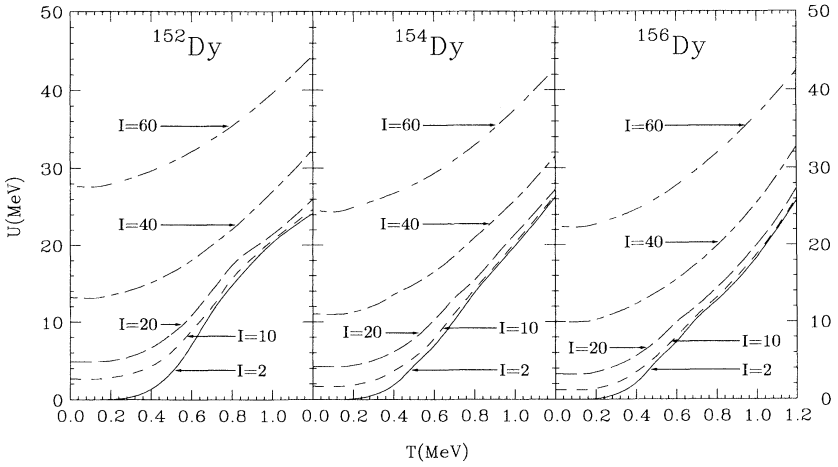

FIG. 1. Internal energy of the nuclei ^{152}Dy, ^{154}Dy, and ^{156}Dy for different angular momenta.

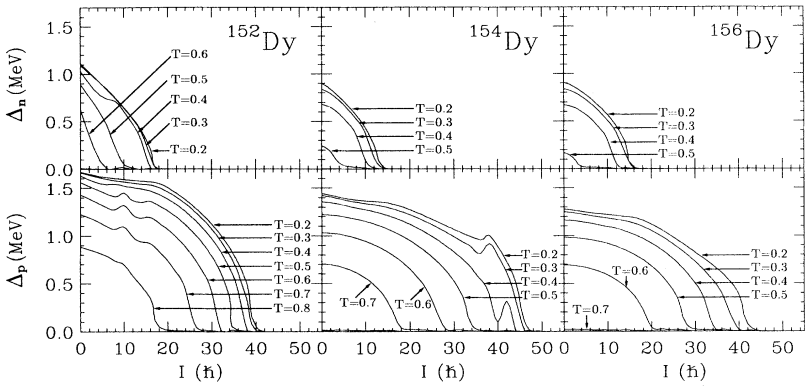

FIG. 2. Energy gaps for the nuclei ^{152}Dy, ^{154}Dy, and ^{156}Dy.

0.7 MeV for the proton system in the same order as before). This twofold transition with growing temperature and increasing angular momentum is in complete analogy to the transition from the superconducting phase to the normal conducting phase in a solid with increasing temperature and with increasing external magnetic field. These two phase transitions have been observed in earlier calculations with similar results to ours [7,9,35,11]. In mean-field calculations these phase transitions are very sharp as in an infinite system. For a finite system, however, one does not expect such types of transitions and, indeed, if one consider further correlations from a quantum origin at zero temperature [36] and from thermal types at finite temperatures [14,37,38] these transitions are washed out.

In Fig. 3 we present the values of the γ deformation (lower panels) and β deformation (upper panels), in the excitation energy (U in MeV) versus angular momentum plane, found in the self-consistent FTHFB theory. In this plot and in the following similar to this one, U denotes the excitation energy above the yrast line. The gray scale in each panel corresponds to values on the scale on the right of the panel; thus, in the case of γ it goes from oblate shape, $-60°$ in our convention (white in the gray scale), to prolate shape, $0°$ (black in the gray scale).[1] Concerning the β scale, the white color is assigned to the smallest and the black one to the largest value that appears in each panel and they may change from nucleus to nucleus. This assignment is done in order to optimize the gray scale for each case. The white lines indicate the separation between each tone of the gray scale. These nuclei are in a transitional region, and the dramatic effect of the Coriolis force and temperature on the shape is clearly displayed in this figure: The nucleus ^{152}Dy is spherical in the ground state ($I = 0, T = 0$); by slightly increasing the excitation energy and the angular momentum it becomes prolate and triaxial but for angular momentum around $14\hbar$ it turns oblate while the deformation parameter β increases. The subtle interplay between pairing correlations, deformation, and temperature can be observed at spin around $8\hbar$. There, with growing temperature the deformation parameter β increases instead of decreasing; this is due to the pairing collapse that is taking place in this temperature range.

The nuclei $^{154-156}$Dy are prolate deformed in the ground state; here a transition to an oblate weak deformed state takes place at spin around $40\hbar$ for ^{154}Dy and at spin around $60\hbar$ for ^{156}Dy. As mentioned in the Introduction, with this Hamiltonian we are not able to describe superdeformed shapes, in particular those experimentally observed in ^{152}Dy [25]. Since we do not look at excitation energies higher than about 18 MeV, we do not observe in any of the three nuclei the transition to oblate noncollective rotation found by Goodman [15,16] in the transitional nucleus ^{158}Yb at energies above 25 MeV. Close to the yrast line we find in ^{152}Dy and ^{152}Dy small triaxialities.

In Fig. 4 we show the self-consistent moment of inertia defined by

$$\mathcal{J} = \frac{\langle \hat{J}_x \rangle_T}{\omega} \tag{27}$$

as a function of the angular momentum for constant temperatures; ω is the angular frequency of Eq. (1). In transitional nuclei, like these under study, the moment of inertia shows large variations which can be caused by shape change, collapse of pairing correlation, or alignment of particles. For small values of temperature and spin we have pairing correlations, which produce the well-known reduction of $\mathcal{J}$ in this region. For small temperatures we find a steep increase in the moment of inertia between $10\hbar$ and $20\hbar$, which is known to be connected with the sudden alignment of a $i_{13/2}$ neutron pair. In the same way the increase between $20\hbar$ and $40\hbar$ observed in $^{154-156}$Dy is related to the alignment of a $h_{11/2}$ pair of protons. For temperatures higher than 0.5 MeV and small spins the pairing correlations are either collapsed or strongly weakened and we observe an increase in $\mathcal{J}$. At higher temperatures and high spins we find values close to the rigid moment of inertia which keep changing in correspondence to the changing shape of the nuclei.

In Fig. 5 we show the entropy versus the temperature

[1]Since in the FTHFB approximation we do not consider shape fluctuations, we do not have γ values extending to 120°; see below.

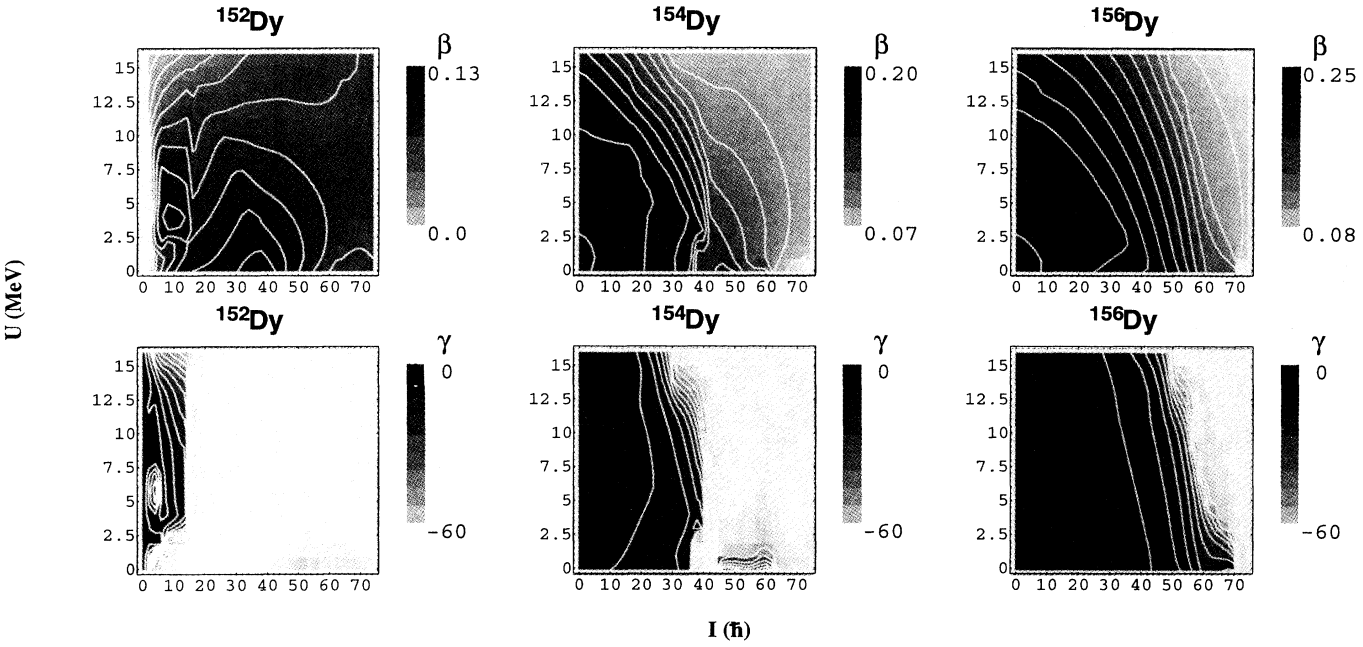

FIG. 3. Self-consistent β-γ values for the nuclei ^{152}Dy, ^{154}Dy, and ^{156}Dy as a function of the excitation energy and the angular momentum.

for constant values of the angular momentum I for the three isotopes. The dependence of the three nuclei is rather similar; they clearly show two distinctive regions, below and above about $T = 0.7$ MeV. Below this temperature we observe, for constant temperature and decreasing angular momentum, a decrease in the entropy. This decline in the entropy is related to the pairing properties discussed in Fig. 2: Higher pairing means increased order and smaller entropy. Above, let us say, $T = 0.7$ MeV, when the pairing correlations have vanished we observe, again for a fixed temperature, the opposite behavior: For increasing angular momentum the entropy decreases. This feature can be understood looking at Fig. 3; if we concentrate, for example, on ^{154}Dy, we see that for fixed excitation energy and increasing angular momentum the nucleus changes from prolate deformed to oblate less deformed, that is, an increase in the symmetry (order) as we increase the angular momentum. This increase in the symmetry again causes a decline in the entropy.

B. Statistical fluctuations

As mentioned in the Introduction, at finite temperature the nucleus performs fluctuations around the most probable configuration. The most relevant fluctuations are those related to the collective degrees of freedom, i.e., the shape parameters (β, γ) — eventually the Euler an-

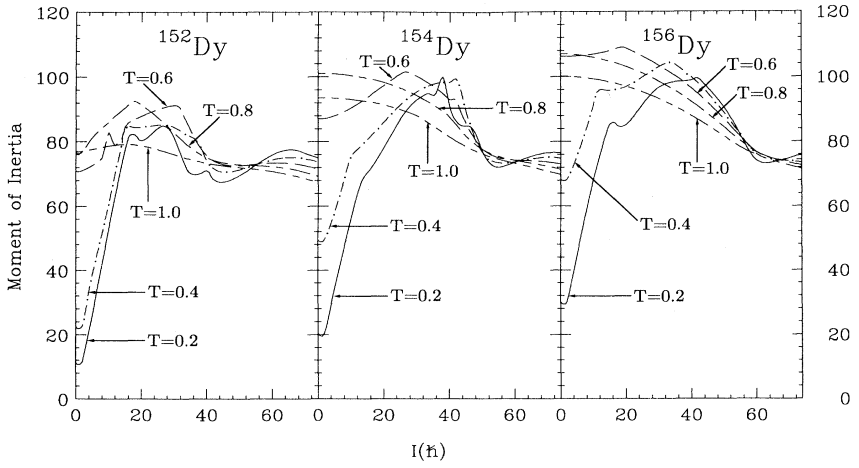

FIG. 4. Moments of inertia (MeV^{-1}) for the nuclei ^{152}Dy, ^{154}Dy, and ^{156}Dy.

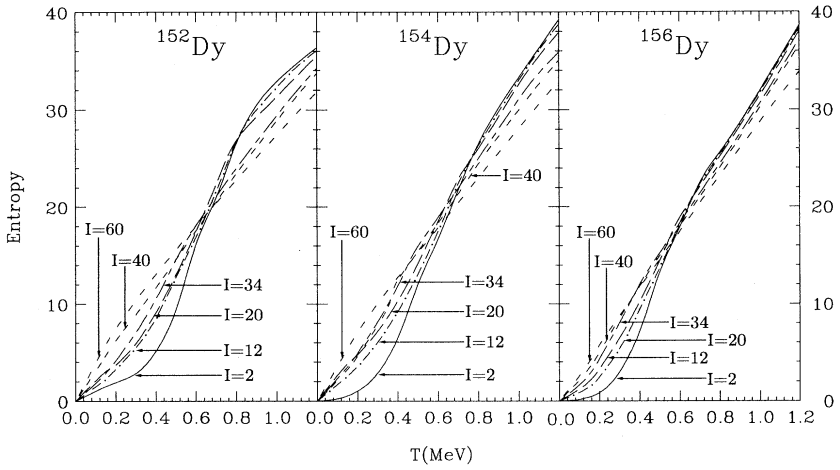

FIG. 5. Entropies of the nuclei ^{152}Dy, ^{154}Dy, and ^{156}Dy as a function of the angular momentum.

gles — and the pairing gap Δ. A microscopic calculation taking into account all these degrees of freedom is not within our capability, and so in this paper we shall concentrate in the role played by the shape fluctuations for the three isotopes ^{152,154,156}Dy. In the calculations that follow we have neglected the pairing correlation, which means that our results are based on the FTHF approximation. If the nucleus performs fluctuations, we have also to consider rotations around different axes. In a calculation with fluctuations the key magnitude is the free energy $F(\beta,\gamma)$ because its exponential provides the weight of each point (β,γ) in the evaluation of expectation values.

To illustrate the situation we display in Fig. 6, as an

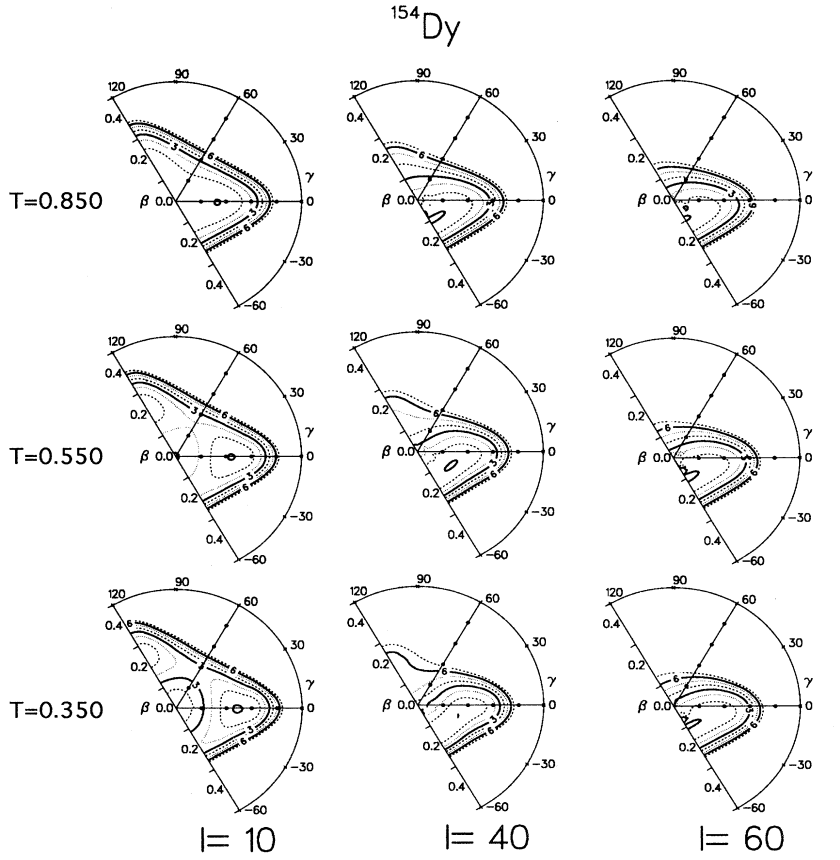

FIG. 6. Free energy for the nucleus ^{154}Dy at selected values of I ($\hbar$) and T (MeV^{-1}) in the β-γ plane. The contour values are given in MeV, the minimum corresponding to zero. The step size is 1 MeV.

example, contour plots of the free energy $F(\beta,\gamma)$ for the nucleus ^{154}Dy in the (β,γ) plane.[2] We use the Hill-Wheeler convention; $\gamma = -60°$ to an oblate shape that rotates around the symmetry axis, $\gamma = 0°$ to a prolate shape that rotates around an axis perpendicular to the symmetry axis, $\gamma = 60°$ to an oblate shape that rotates around an axis perpendicular to the symmetry axis, and $\gamma = 120°$ to a prolate shape that rotates around the symmetry axis. The plots correspond to the following (I,T) values: In the lower row for constant temperature $T = 0.35$ MeV and for values of the angular momentum, from left to right, of $I = 10\hbar, 40\hbar$, and $60\hbar$, in the middle row for the same values of the angular momentum but for $T = 0.55$ MeV, and in the upper row for $T = 0.85$ MeV. These spin values correspond, respectively, to values before, at, and after the phase transition has taken place.

At $T = 0.35$ MeV and $I = 10\hbar$, the absolute minimum corresponds to a prolate shape ($\beta = 0.3$); we also find a maximum close to the spherical shape and a local minimum at $\beta = 0.3$, $\gamma = 120°$. If we concentrate on the first column, we can observe the effect of temperature for $I = 10\hbar$; by increasing temperature we find a twofold effect, the softening of the surface in the γ direction (the local minima have been washed out) and the shifting of the absolute minimum towards spherical shapes. The effect of increasing the angular momentum (we now concentrate on a row) is to inhibit rotations around $\gamma = 120°$ (at this γ value the rotational energy calculated with the rigid moment of inertia is a maximum for constant β), the rotational energy driving the system to slightly oblate-prolate shapes at low temperatures and to slightly oblate-spherical shapes at higher temperatures as we would expect for a classical system.

In the first column of Fig. 7 we show the most probable deformation parameters β, upper part, and γ, lower part, in the plane excitation energy, and angular momentum for the nucleus ^{152}Dy, calculated in the FTHF approximation. These results are the equivalent of the first column of Fig. 3; the only difference is that in this figure, as mentioned, we have neglected the pairing correlations. The main difference appears at low spin and low excitation energies; here we find the nucleus to be prolate deformed at variance with Fig. 3 where we find it to be spherical. In transitional nuclei, obviously, the effect of the pairing correlation may be very important. At moderate excitation energies and high angular momentum we expect, however, the same results in both

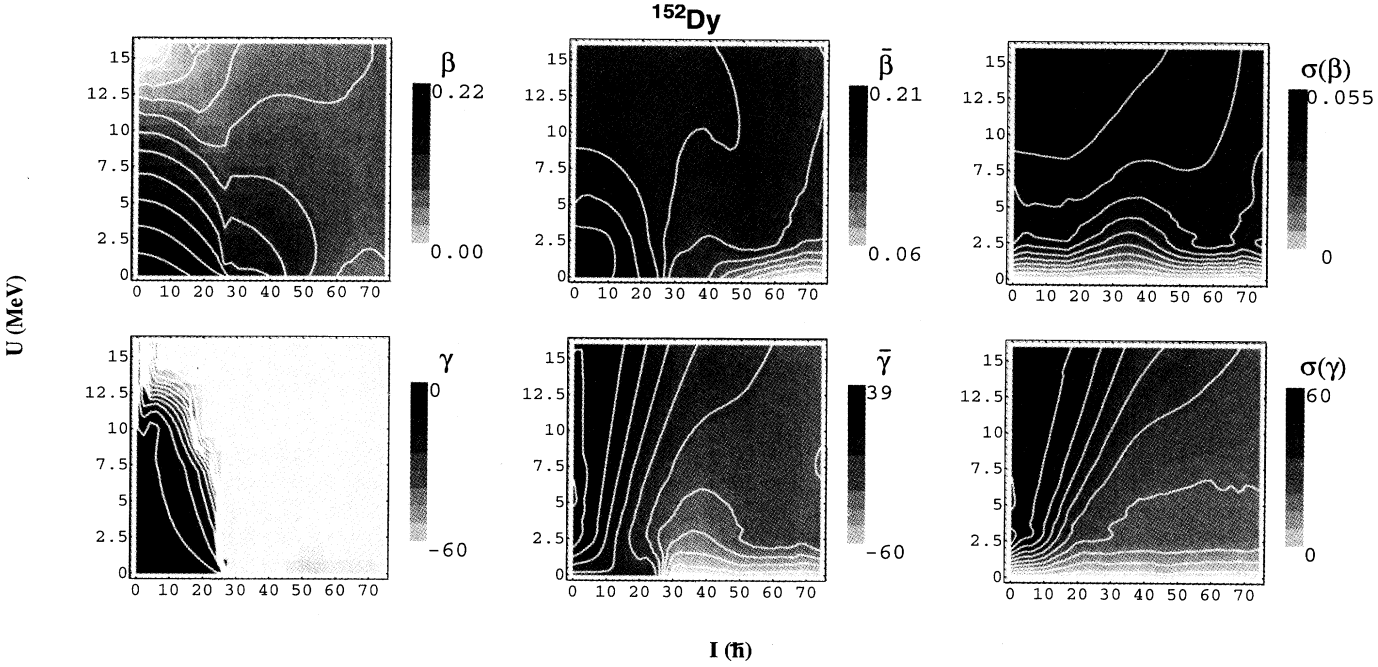

FIG. 7. Self-consistent deformations parameters (β,γ), average values $(\bar{\beta},\bar{\gamma})$, and deviations $[\sigma(\beta),\sigma(\gamma)]$ for the nucleus ^{152}Dy.

[2]The free energy surfaces of ^{152}Dy, ^{154}Dy, and ^{156}Dy, though *quantitatively* different, display in a unique way the important physics at large spins and high excitation energies. For this reason, and in order to save space, we shall only display the one for ^{154}Dy. We will refer, therefore, to this figure to discuss global *qualitative* properties of all three dysprosium isotopes.

calculations. This is found to be the case, as can be seen in the contour lines for β and γ.[3] The white band in the γ plot at $I \approx 26\hbar$ is caused by an accumulation of white lines, indicating a very sharp change in γ. In the middle column we show, for the same nucleus, the average values $\bar{\beta}$, upper part, and $\bar{\gamma}$, lower part, as defined in Eq. (21). For small excitation energies, i.e., in the vicinity of the yrast line, we find, as expected, values of $\bar{\beta}$ and $\bar{\gamma}$ very similar to the self-consistent values β and γ. At higher excitation energies we find strong discrepancies, especially in $\bar{\gamma}$; only close to the yrast line do we find values of $\bar{\gamma}$ near $-60°$. In general, we find extended regions of large triaxialities especially at not very high angular momentum; oblate or nearly oblate shapes are only found close to the yrast line at high angular momentum.

Concerning the $\bar{\beta}$ values we find the effect of thermal averaging smaller as compared with $\bar{\gamma}$; this can be easily understood from Fig. 6, where we see that the energy surface is much softer in the γ direction than in the radial (β) direction. Another reason why the thermal averaging on β is not as spectacular as with γ is due to the fact that in the range of temperatures in which we are interested in the present paper, we have not reached yet the transition to $\beta = 0$. We also find that the average deformation, in general, diminishes when we increase the angular momentum and/or the excitation energy. Last, in the third column of Fig. 7, the standard deviation $\sigma(\beta)$, upper part, and $\sigma(\gamma)$, lower part, as defined in Eq. (22), are represented. We find large values of $\sigma(\beta)$, these values increasing, obviously, with the temperature. For relatively high constant values of the excitation energy and growing values of the angular momentum we find a decrease of $\sigma(\beta)$ due to the above-mentioned fact of the inhibition of rotation with large β values for $\gamma = 120°$ at large angular momentum. As expected, at very low excitation energies the standard deviation goes to zero. We also find large values of $\sigma(\gamma)$, ranging from 0° to 60°. Similar results have been found by Goodman (see [3] and references therein) for specific values of the angular momentum and temperature. The standard deviation $\sigma(\gamma)$ grows with temperature and diminishes with increasing angular momentum. This pattern can be understood by looking again at Fig. 6, for example, at $T = 0.550$, for the three values of the angular momentum. For $I = 10\hbar$ we find contours between 1 and 2 MeV for γ values ranging from $-60°$ to $+120°$, for $I = 40\hbar$ the same contour goes from $-60°$ up to approximately 10°, and for $I = 60\hbar$, however, the same contour covers again the whole γ range.

The calculations for the nucleus ^{154}Dy show that, as with the nucleus ^{152}Dy, the self-consistent γ degree of freedom is much softer concerning the angular momentum than the excitation energy. The mean-field prediction for the transition to oblate shapes takes place in this isotope at $I \approx 40\hbar$, though some triaxialities remain at higher angular momentum and low excitation energies. The self-consistent β values in this nucleus are larger than in ^{152}Dy; the softness of the β degree of freedom with respect to the spin and excitation energy dependence is, to some extent, similar. The average γ values, $\bar{\gamma}$, present very extended regions of triaxial shapes; we find some close to oblate shapes at low energies and around spin values $50\hbar$ and $70\hbar$. The average β values, $\bar{\beta}$, are larger and the surface stiffer against temperature changes than in the ^{152}Dy nucleus. The standard deviations $\sigma(\gamma)$ and $\sigma(\beta)$ display similar characteristics to the previous nucleus.

Concerning ^{156}Dy, we observe a consolidation of the tendency found in the nucleus ^{154}Dy; i.e., the nucleus behaves as a good rotor rather stiff against excitation energy and angular momentum. We find γ values close to $-60°$ only at the very high spins ($I \approx 60\hbar$) and the overall deformation is larger than in the previous nuclei.

In Fig. 8 we show, in the first column, the reduced transition probability in the mean-field approximation [$B(E2)$] [see Eq. (23)] for the nuclei ^{152}Dy, ^{154}Dy, and ^{156}Dy from top to bottom, respectively. In the ordinate axis of each box we plot again the excitation energy and in the abscissas the angular momentum. In Ref. [39] it has been shown that at finite temperature the transition probabilities behave like $\beta^2 \cos^2(30° - \gamma)$, which means that the lines of equal transition probability are, in the (β, γ) plane, parallel to the diameter determined by the $\gamma = -60°$ radius and the $\gamma = 120°$ one. The contour lines are, therefore, straight lines parallel to this diameter; on the diameter they are zero, taking growing values as they move away from it. In Fig. 8 we clearly see how the collectivity develops from ^{152}Dy to ^{156}Dy, both in intensity and in extension in the (U, I) plane; the regions with $B(E2) \approx 0$ correspond to the ones with $\gamma \approx -60°$ as can be seen in Fig. 7 for the ^{152}Dy case. In the second column the average reduced transition probability $\overline{B}(E2)$, as defined in Eq. (21), is presented for the same nuclei and in the same order as before. The effect of the thermal fluctuations is an increase of the overall collectivity; in particular for the regions of the (U, I) plane where we get zero in the mean-field approximation we now obtain about 110 W.u. for ^{152}Dy, 140 W.u. for ^{154}Dy, and 170 W.u. for ^{156}Dy.

In the third column of the same figure the standard deviations of the average reduced transition probabilities, $\sigma(B(E2))$, as defined in Eq. (22), are depicted. Here again large deviations, increasing from ^{152}Dy to ^{156}Dy, are found. The pattern in all three nuclei is qualitatively similar; first, the horizontal contour lines at the bottom, second, the perpendicular contour lines at moderate and high spin, and third the maximum value of the standard fluctuations are located at very small angular momentum and moderate excitation energy. The horizontal lines at the bottom represent the usual increase in the fluctuations accompanying the increase of temperature. The other two effects can be easily understood considering the lines of equal transition probability as described above and the free energy surfaces (Fig. 6). At high spin (see the third column of Fig. 6) we have extended minima close to the oblate axis with small or no

[3] In order to compare different plots of this kind one should keep in mind that the gray tonalities are not absolute but they are referred to the bar at the right of each figure.

contribution to the $B(E2)$; the lines with the largest contribution are those far away from the above-mentioned diameter, but these lines look very similar for fixed angular momentum and growing temperature. That means that we expect the same values for $\sigma(B(E2))$ for constant angular momentum; i.e., the contour lines will be perpendicular to the spin axis. The behavior at small angular momentum with growing temperature differs from the high-spin one by the fact that temperature effects are dominant. It is also easy to pin down: The increase at small excitation energies we have already discussed; the maximum in the standard deviation is reached by temperatures high enough to make the fluctuations important but low enough that the shell structure is not washed out. At higher temperatures the nucleus will be driven to less deformed shapes (see the first column of Fig. 6) with the corresponding decrease in the $B(E2)$ values.

In Fig. 9, last, we show in a similar display as in Fig. 8, in the first column the self-consistent moment of inertia, $\mathcal{J}$, as defined in Eq. (27). In the three cases we observe an accumulation of lines at low excitation energies due to the alignment of particles in the $\nu i_{13/2}$ and $\pi h_{11/2}$ orbitals. The self-consistent moments of inertia, again in all three nuclei, are large for those parts of the (U, I) plane where the shell effects are important (see Fig. 7); at very high angular momentum and/or high excitation energies we get values close to the rigid moment of inertia. In the middle column, the thermal-averaged moments of inertia are displayed. The trend, as shown by the contour lines, is also similar in all three nuclei: The largest values are for small temperatures and medium angular momenta; by increasing the excitation energy and increasing or decreasing spins, $\bar{\mathcal{J}}$ diminishes. That means that, for constant energy (at not too high values) and growing angular momentum, we expect $\bar{\mathcal{J}}$ first to grow and later on, for large enough spins, to decrease. This behavior can be understood by looking at the free energy of Fig. 6. Let us concentrate on the middle row of this figure. Here we find, for $I = 10\hbar$, contour lines, with the value 1, for example, populating the $\gamma = 120°$ axis. In our convention the moment of inertia takes its smallest

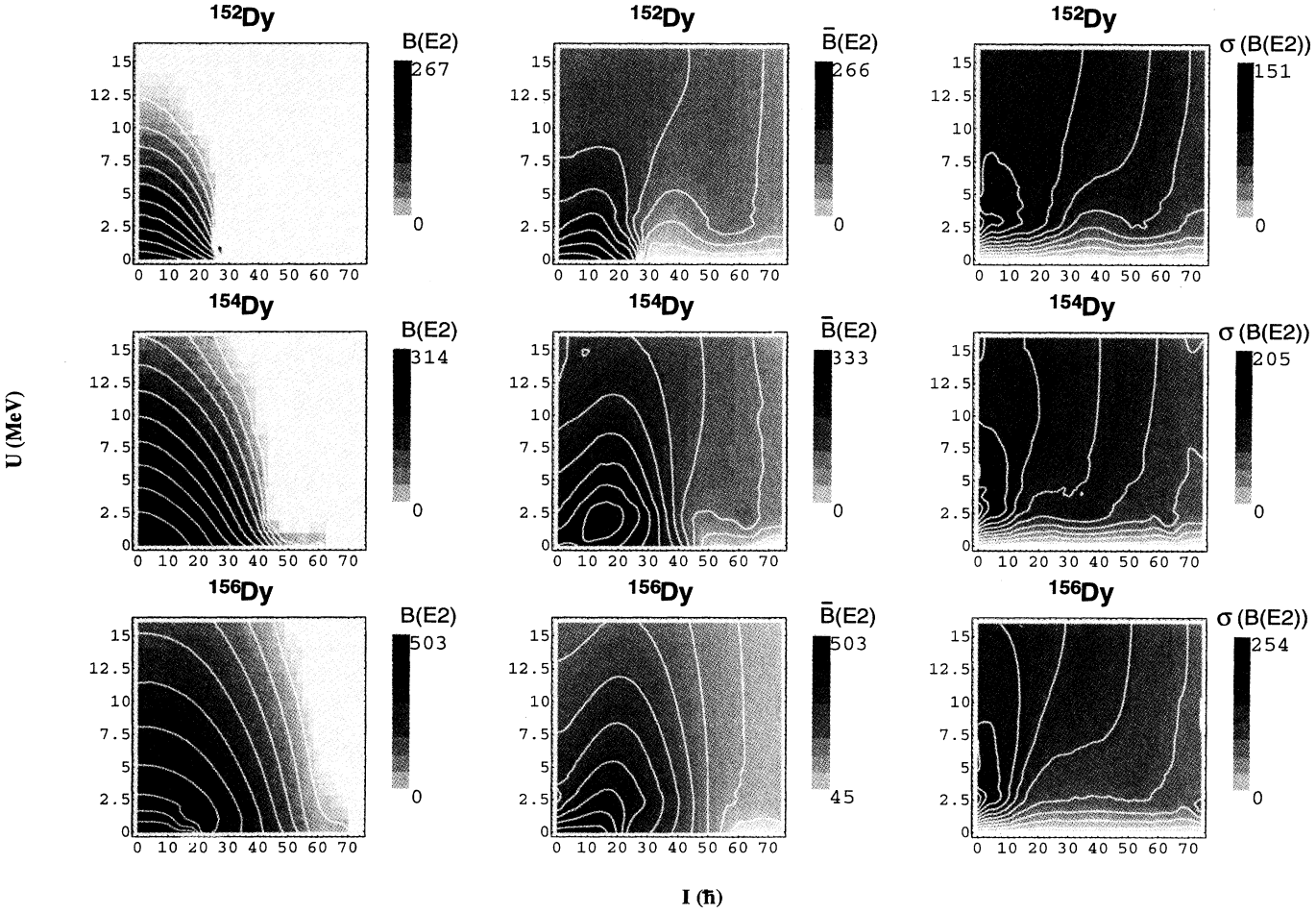

FIG. 8. Self-consistent reduced transition probabilities $B(E2)$ (W.u.), average values $[\bar{B}(E2)]$, and deviations $[\sigma(B(E2))]$, for the nuclei ^{152,154,156}Dy.

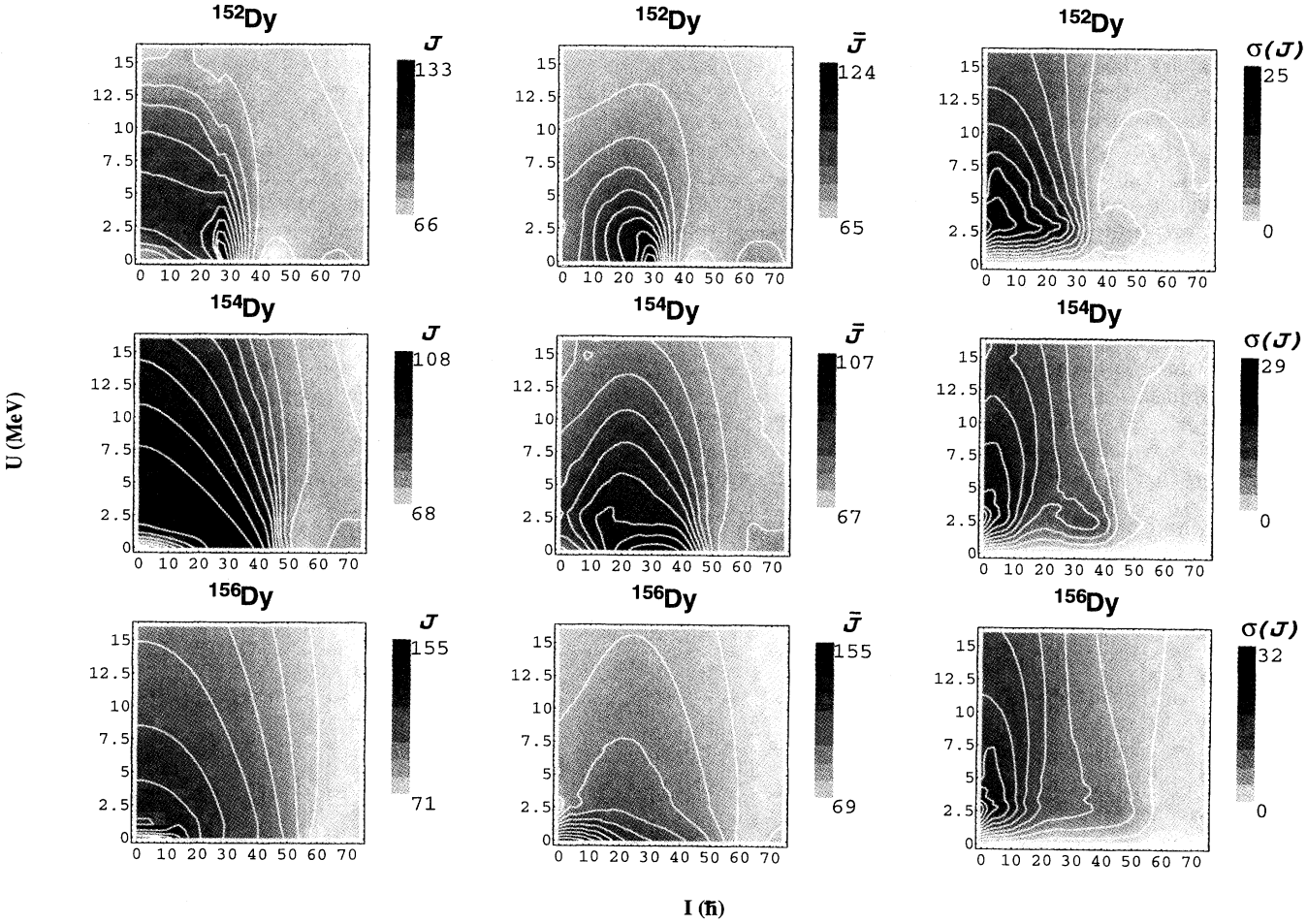

FIG. 9. Self-consistent moments of inertia, $\mathcal{J}$ (MeV^{-1}), average values ($\bar{\mathcal{J}}$), and deviations [$\sigma(\mathcal{J})$], for the nuclei ^{152,154,156}Dy.

value at this axis. For $I = 40\hbar$ we populate mainly triaxial shapes; we expect, therefore, large moments of inertia. For $I = 60\hbar$ we see the probability distribution centered at $\gamma = -60°$, and somewhat smaller β deformation as before; i.e., we expect a decrease in the average moment of inertia as compared with the previous case. In the third column we present the standard deviations of the moments of inertia. They are large and their behavior can be understood by using similar arguments as those used in the discussion of the two previous columns.

IV. CONCLUSIONS

We have performed a systematic study of the dysprosium isotopes within the framework of the cranked finite-temperature Hartree-Fock-Bogoliubov theory. We have used the pairing-plus-quadrupole Hamiltonian and the configuration space of Baranger and Kumar as well as their force strengths. We have studied the quasicontinuum up to 16 MeV excitation energy and up to spin values of $I = 70\hbar$.

These nuclei are in a transitional region and one expects shape fluctuations, both quantum and thermal, to be important. At high excitation energies one expects the thermal fluctuations to be dominant. We have taken them into account in the frame of classical statistics. We have found a very rich structure in all observables as a function of the angular momentum and the temperature. In the mean-field approximation a sharp phase transition from prolate to oblate nuclei is found. The inclusion of thermal fluctuations washes out the phase transition already at a relatively low temperature.

ACKNOWLEDGMENTS

We would like to thank the staff at the computing facility of the Facultad de Informatica of the Universidad Politécnica de Madrid for their technical support. This work was supported in part by DGICyT, Spain under Project PB91-0006.

[1] J.C. Bacelar *et al.*, Phys. Rev. Lett. **56**, 1858 (1985).
[2] J.E. Draper *et al.*, Phys. Rev. Lett. **56**, 309 (1986).
[3] A.L. Goodman, in *Nuclear Physics at the Borderlines*, edited by J.M. Arias *et al.* (Springer-Verlag, Berlin, 1991), p. 94.
[4] J.L. Egido and P. Ring, J. Phys. G **19**, 1 (1993).
[5] J. des Cloizeaux, in *Many-Body Physics*, edited by C. de Witt and R. Balian (Gordon and Breach, New York, 1968).
[6] M. Brack and P. Quentin, Phys. Lett. **52B**, 156 (1974).
[7] A.L. Goodman, Nucl. Phys. **A352**, 30, 45 (1981).
[8] M.E. Faber and M. Ploszajczak, Z. Phys. A **291**, 331 (1979).
[9] K. Tanabe, K. Sugawara-Tanabe, and H.J. Mang, Nucl. Phys. **A357**, 20 (1981); **A357**, 45 (1981).
[10] A.L. Goodman, Nucl. Phys. **A369**, 365 (1981); **A370**, 90 (1981).
[11] J.L. Egido, P. Ring, and H.J. Mang, Nucl. Phys. **A451**, 77 (1986).
[12] Y. Alhassid, B. Bush, and S. Levit, Phys. Rev. Lett. **61**, 1929 (1988).
[13] Y. Alhassid and B. Bush, Nucl. Phys. **A509**, 461 (1990).
[14] L.G. Moretto, Phys. Lett. **44**, 494 (1973).
[15] A.L. Goodman, Phys. Rev. **39**, 2478 (1989).
[16] A.L. Goodman, Nucl. Phys. **A504**, 413 (1989).
[17] R. Holzmann *et al.*, Phys. Lett. B **195,** 321 (1987).
[18] R. Holzmann *et al.*, Phys. Rev. Lett. **62,** 520 (1989).
[19] Y. Alhassid, in *New Trends in Nuclear Collective Dynamics*, Springer Proceedings in Physics, Vol. 58, edited by Y. Abe, H. Horiuchi, and K. Matsuyanagi (Springer-Verlag, New York, 1991), pp. 41–90.
[20] M. Gallardo, M. Diebel, T. Dossing, and R.A. Broglia, Nucl. Phys. **A443**, 415 (1985).
[21] J.L. Egido, C. Dorso, J.O. Rasmussen, and P. Ring, Phys. Lett. B **178**, 139 (1986).
[22] K. Kumar and M. Baranger, Nucl. Phys. **A110**, 529 (1968).
[23] J.L. Egido, H.J. Mang, and P. Ring, Nucl. Phys. **A334**, 1 (1980).
[24] J.L. Egido, H.J. Mang, and P. Ring, Nucl. Phys. **A339**, 390 (1980).
[25] P. Twin and P. Nolan, Annu. Rev. Nucl. Part. Sci. **38**, 533 (1988).
[26] A.L. Goodman, in *Advances in Nuclear Physics*, edited by J. Negele and E. Voigt (Plenum, New York, 1979), Vol. II.
[27] A.V. Ignatyuk, I.N. Mikhailov, L.M. Molina, R.G. Nazmitdinov, and K. Pomorsky, Nucl. Phys. **A346**, 191 (1980).
[28] L.D. Landau and E.M. Lifshitz, *Course of Theoretical Physics* (Pergamon Press, Oxford, 1959).
[29] A.L. Goodman, Phys. Rev. C **38**, 1092 (1988).
[30] J.L. Egido and H.A. Weidenmüller, Phys. Rev. C **39**, 2398 (1989).
[31] A.L. Goodman, Nucl. Phys. **A230**, 466 (1974).
[32] I. Ragnarsson, in conference report to the XXIII Zakopane School of Physics, Zakopane, Poland, 1988 (unpublished).
[33] I. Ragnarsson, Phys. Lett. B **217**, 33 (1989).
[34] A.L. Goodman, Nucl. Phys. A (to be published).
[35] P. Ring, L.M. Robledo, J.L. Egido, and M. Faber, Nucl. Phys. **A419**, 261 (1984).
[36] J.L. Egido and P. Ring, Nucl. Phys. **A388**, 19 (1989).
[37] A.L. Goodman, Phys. Rev. C **29**, 1887 (1984).
[38] J.L. Egido, P. Ring, S. Iwasaki, and H.J. Mang, Phys. Lett. **154B**, 1 (1985).
[39] J.L. Egido, Phys. Lett. B **232**, 1 (1989).

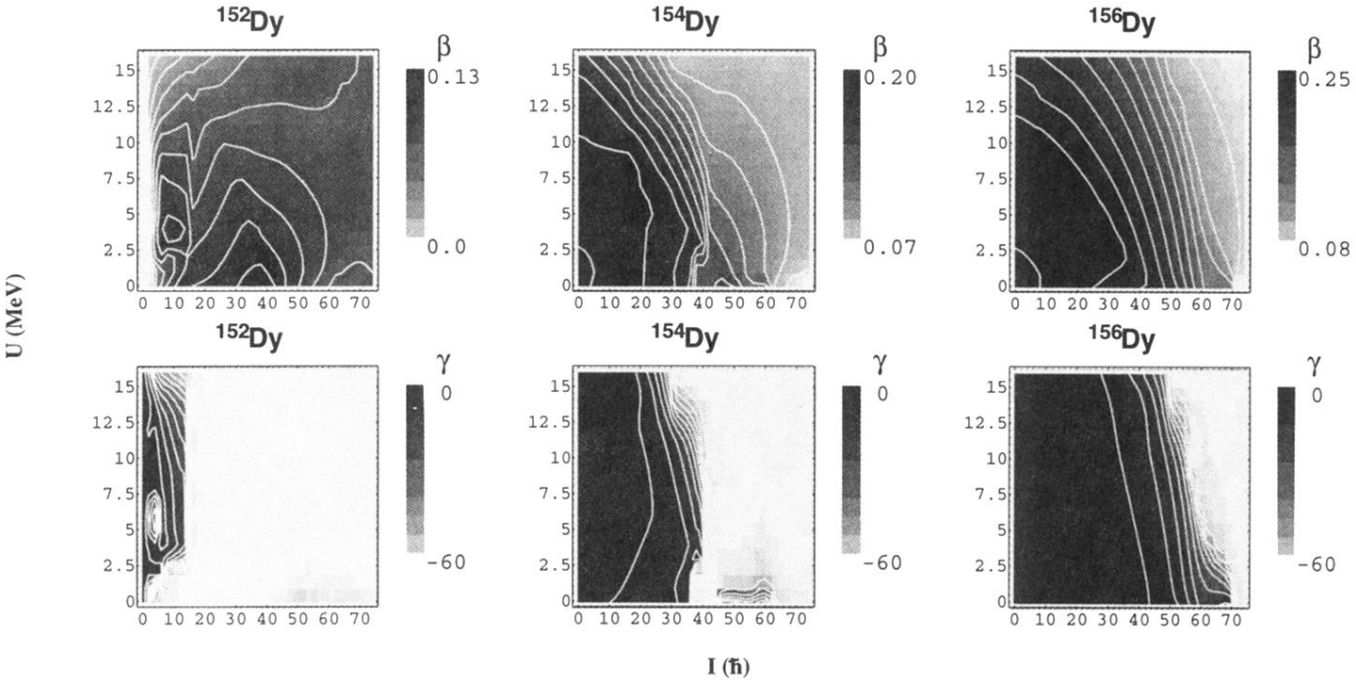

FIG. 3. Self-consistent β-γ values for the nuclei ^{152}Dy, ^{154}Dy, and ^{156}Dy as a function of the excitation energy and the angular momentum.

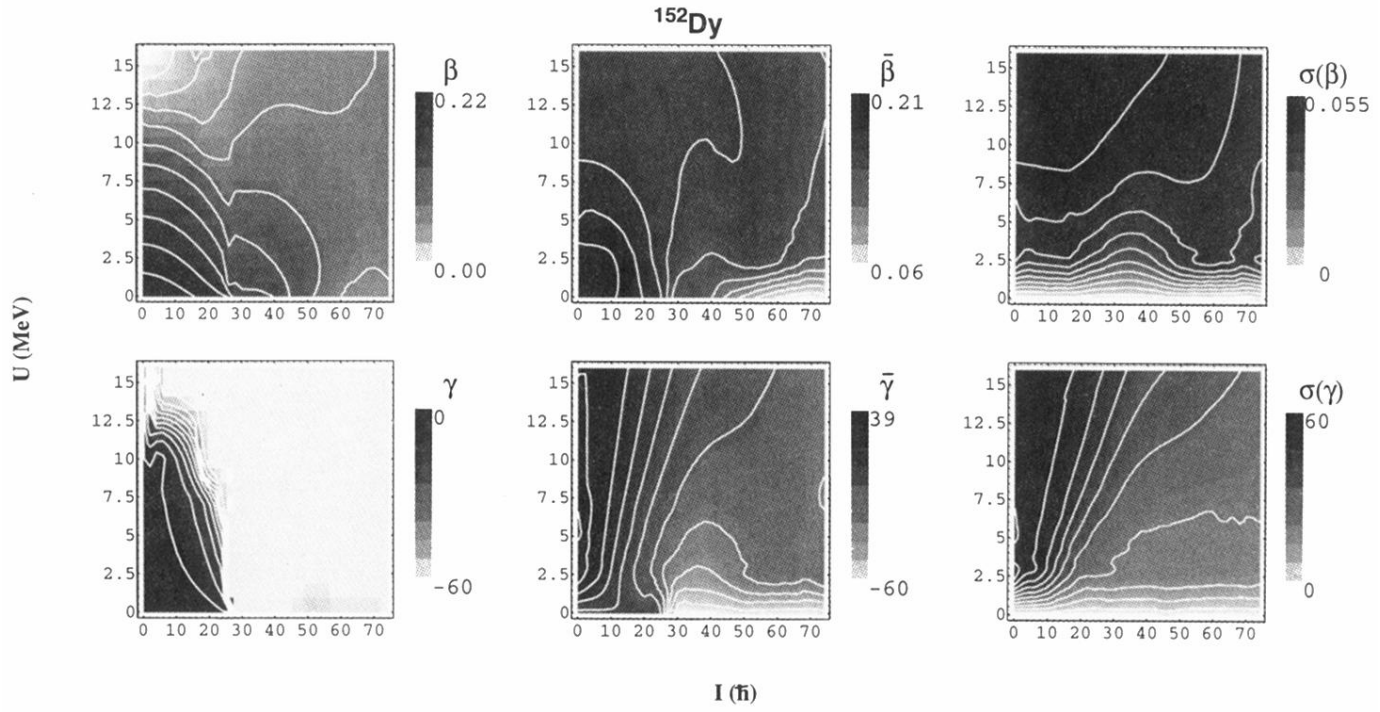

FIG. 7. Self-consistent deformations parameters (β, γ), average values $(\bar{\beta}, \bar{\gamma})$, and deviations $[\sigma(\beta), \sigma(\gamma)]$ for the nucleus ^{152}Dy.

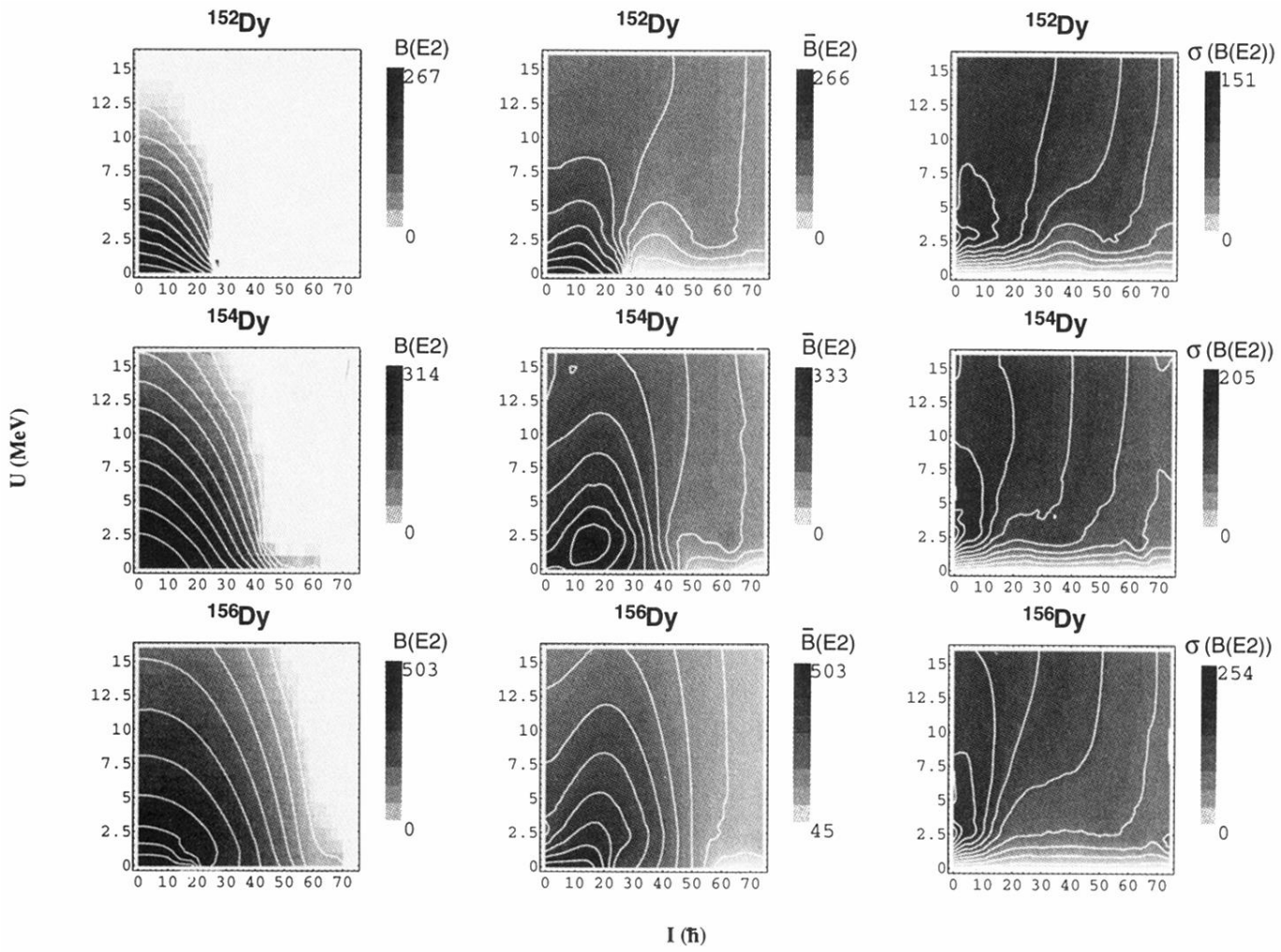

FIG. 8. Self-consistent reduced transition probabilities $B(E2)$ (W.u.), average values $[\bar{B}(E2)]$, and deviations $[\sigma(B(E2))]$, for the nuclei ^{152,154,156}Dy.

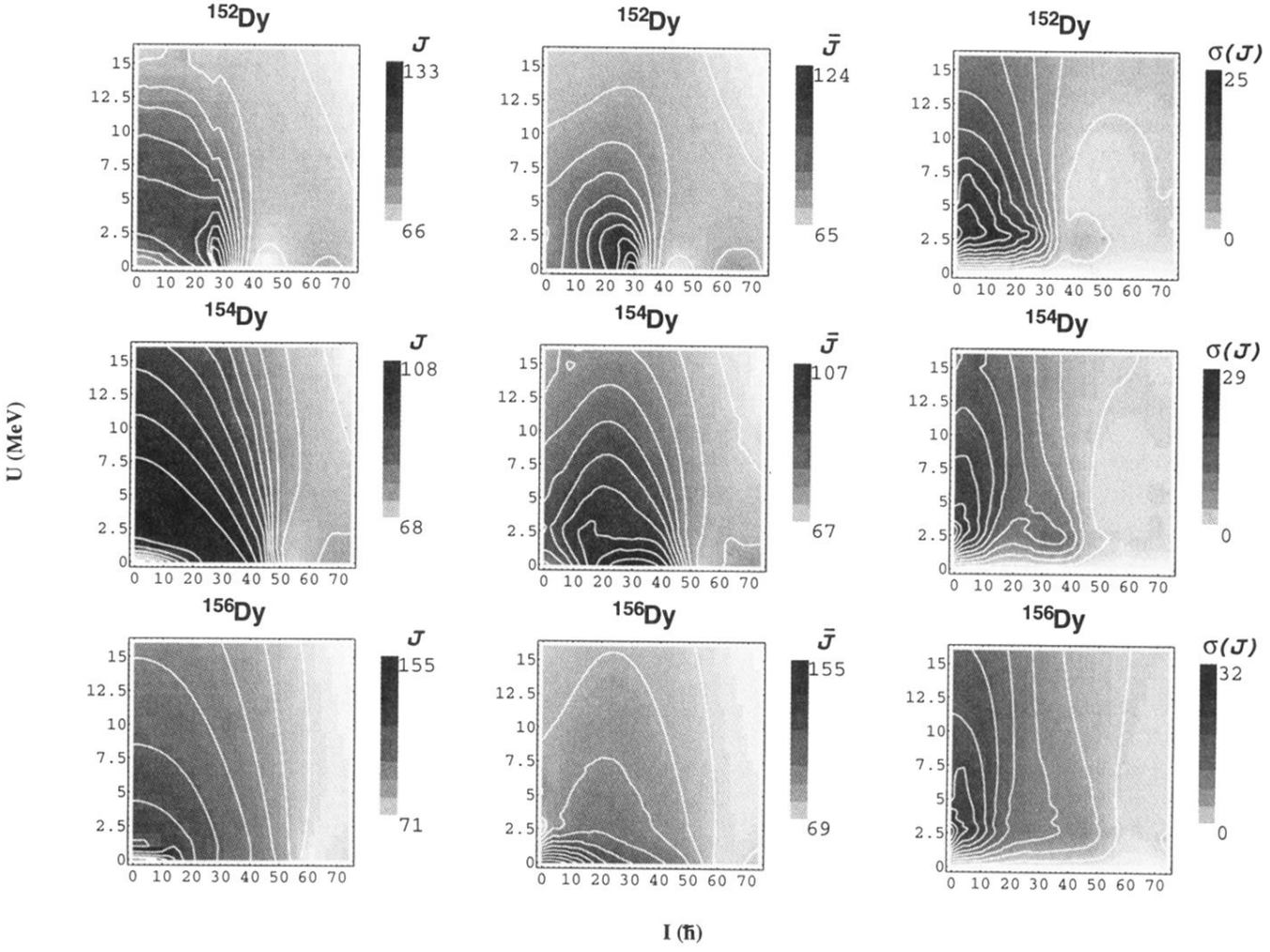

FIG. 9. Self-consistent moments of inertia, $\mathcal{J}$ (MeV^{-1}), average values ($\bar{\mathcal{J}}$), and deviations [$\sigma(\mathcal{J})$], for the nuclei ^{152,154,156}Dy.